journal homepage: www.intl.elsevierhealth.com/journals/cmpb

An integrative software package for gastrointestinal biomagnetic data acquisition and analysis using SQUID magnetometers

Andrei Irimia[a,*], *Leo K. Cheng*[b], *Martin L. Buist*[b], *Andrew J. Pullan*[b,c], *L. Alan Bradshaw*[a]

[a] *Living State Physics Laboratories, Department of Physics and Astronomy, Vanderbilt University, Nashville, TN 37235, USA*
[b] *Bioengineering Institute, University of Auckland, Auckland, New Zealand*
[c] *Department of Engineering Science, University of Auckland, Auckland, New Zealand*

ARTICLE INFO

Article history:
Received 4 December 2004
Received in revised form
26 January 2006
Accepted 6 March 2006

PACS:
87.17.Aa
87.18.Bb

Keywords:
Gastric electrical activity
Intestinal electrical activity
Signal acquisition
Signal processing
Software package
Magnetogastrography
Magnetogastrogram
Data analysis

ABSTRACT

The study of bioelectric and biomagnetic activity in the human gastrointestinal (GI) tract is of great interest in clinical research due to the proven possibility to detect pathological conditions thereof from electric and magnetic field recordings. The magnetogastrogram (MGG) and magnetoenterogram (MENG) can be recorded using superconducting quantum interference device (SQUID) magnetometers, which are the most sensitive magnetic flux-to-voltage converters currently available. To address the urgent need for powerful acquisition and analysis software tools faced by many researchers and clinicians in this important area of investigation, an integrative and modular computer program was developed for the acquisition, processing and analysis of GI SQUID signals. In addition to a robust hardware implementation for efficient data acquisition, a number of signal processing and analysis modules were developed to serve in a variety of both clinical procedures and scientific investigations. Implemented software features include data processing and visualization, waterfall plots of signal frequency spectra as well as spatial maps of GI signal frequencies. Moreover, a software tool providing powerful 3D visualizations of GI signals was created using realistic models of the human torso and internal organs.

1. Introduction

The study of the electrical control activity (ECA) in the stomach is of great interest in the medical field due to the proven possibility to detect various pathological conditions of this organ from the analysis of gastrointestinal slow wave signals. Although over 60 million Americans are affected by digestive diseases [9], the electrophysiological mechanisms associated with pathological conditions in the gastrointestinal system are only beginning to be understood. One such condition is gastroparesis, which is characterized by abnormally slow gastric emptying rates, dyspepsia, nausea, discomfort and intermittent vomiting [17,22]. In the past, numerous investigations were carried out to detect phenomena associated with diseases such as gastroparesis and ischemia using the electrogastrogram (EGG) and magnetogastrogram (MGG) [8]. Given that

* *Corresponding author.*
0169-2607/$ – see front matter © 2006 Elsevier Ireland Ltd. All rights reserved.
doi:10.1016/j.cmpb.2006.03.006

the mortality rate of patients suffering from acute mesenteric ischemia – including mesenteric venous thrombosis (MVT) – is at least 50%, the importance of such studies cannot be overstated.

The gastric slow wave, first recorded in 1921 by Alvarez [1], is a biophysical phenomenon that originates in the corpus of the stomach and propagates across this organ in the form of a de-polarization/re-polarization wave front moving toward the pylorus at a frequency of three to four cycles per minute (cpm) in human subjects. Electric propagation is made possible by the smooth gastric muscle, which consists of several layers of coupled cells that allow polarization waves to advance across the stomach until they reach the pylorus. At that point, propagation resets to the corpus region before a new cycle begins.

Because abnormalities in the propagation of GI bioelectric currents are associated with disease states, a great deal of investigative effort has been invested in the direction of detecting them noninvasively. Experimentally, bioelectric currents have been detected and investigated using the EGG; in recent years, however, a number of inherent difficulties associated with this method – such as the dependence of electric recordings upon tissue conductivity, which attenuates the EGG signal – have suggested the use of the magnetogastrogram (MGG) instead, because the magnetic – and not electric – field of the stomach is measured with the latter procedure. This is advantageous because magnetic fields are dependent on tissue permeability, which is nearly equal to that of free space. Investigating the GEA from magnetic field recordings is also encouraging due to the finding that, although magnetic field strengths decrease rapidly with distance from their sources, they do reveal the characteristics of these sources in a more accurate manner [3,4].

Due to the fact that gastric biomagnetic fields have very weak strength-of the order of 10^{-12} T-a highly sensitive measurement apparatus is required for experimental data collection. Such an instrument is the superconducting quantum interference device (SQUID) biomagnetometer, which remains to this date the most sensitive device for the detection and measurement of extremely low-magnitude magnetic fields. In particular, the Tristan 637i biomagnetometer, produced by Tristan Technologies (San Diego, CA), is a highly sensitive, multichannel SQUID magnetometer system that can detect the bioelectromagnetic activity in the human stomach and intestine. Among others, the SQUID magnetometer has been shown to possess the ability of detecting intestinal ischemia, a disease that is difficult to diagnose and usually fatal. SQUID sensors are able to detect signals resulting from the basic electrical rhythm (BER) of the intestine, whose frequency changes under ischemia. Thus, the potential for the use of SQUIDs in clinical diagnosis is significant.

For a number of years, SQUID magnetometers have been used very successfully to detect and study GI diseases. Nevertheless, although the hardware components of this instrument are available commercially as an integrated unit, the same cannot be said about the numerous software tools that are often required for processing and analyzing SQUID data. Such tools are nevertheless indispensable to a large variety of clinicians, engineers and biophysicists whose work involves the analysis of GI biomagnetic signals. In spite of this acute need, an integrative, user-friendly software tool for acquiring and analyzing GI SQUID data has not yet appeared in the scientific literature. In order to fulfill the need for such a computer-based system, a modular, integrative and multipurpose software program has been designed, implemented and tested on the SQUID 637i biomagnetometer produced by Tristan Technologies (San Diego, CA). The purpose of this article is to describe this integrative software and to demonstrate its suitability and usefulness to clinical research. Moreover, one goal of the work described in what follows is to set the standard for SQUID data processing software and to significantly improve the state of the art in the important and critical research area of biomagnetic instrumentation and analysis.

The computer software program presented in this article makes extensive use of an advanced modeling tool called 'Continuum Mechanics, Image analysis, Signal processing and System identification' (CMISS). CMISS is a 3D modeling environment developed by the Bioengineering Institute at the University of Auckland (Auckland, New Zealand). The purpose of this software is to provide a set of tools for applying the boundary element method (BEM) and finite element method (FEM) to a variety of problems in bioengineering, such as cardiac and GI biopotential problems. It consists of a number of modules including a graphical front end with advanced 3D display and modelling capabilities, and a computational back end that can be executed remotely on powerful workstations or supercomputers [7]. The CMISS graphical user interface (GUI) consists of an input box where CMISS commands can be entered, a panel where the content of these commands is stored throughout each user session, and a second panel where feedback is provided to the user by CMISS with respect to the execution of the commands that were entered. The interface also provides a series of menus for loading commands from input files with the `.com` extension and for performing a number of various graphical and computational tasks.

After significant contributions to the Cardiome project, the Bioengineering Group at the University of Auckland laid the foundation of the Gut Physiome project, which involves the development of a modeling framework that integrates physiological, anatomical and medical knowledge of the GI system. Equations derived from physical conservation laws are solved in CMISS to predict the integrative behaviour of an organ from knowledge of the anatomical structure and tissue properties. The tissue properties used in these organ level simulations can also incorporate tissue structure and cellular processes such as ion movement through membrane channels, signal transduction pathways and metabolic processes, together with the spatial variation of the parameters characterizing these processes. CMISS has facilities for fitting models to geometric data from imaging modalities such as magnetic resonance imaging (MRI) or computed tomography (CT) and has a rich set of tools for graphical interaction with the models and the display of simulation results. Control of the program is via GUIs or scripting languages such as Perl and Python.

The main academic goal of CMISS is to support the Physiome project of the International Union for Physiological Sciences (IUPS) [15]. This requires the ability to model biological structure and function at all scales from the molecular structure of proteins (nm scale) to 3D cell models (μm) to tissue models (mm) to whole organ models (m), and the ability to relate models at widely different temporal scales. The compu-

tational engine encompasses a number of computational algorithms designed to handle the particular problems of modelling biological structures and systems. The computational and graphical engines can be invoked either together or separately so large computational tasks can be performed on supercomputers and the visualization of results can be done on a graphics workstation. The code base is designed to have a minimum of architecture specific routines allowing CMISS to run on multiple UNIX-based platforms including Linux on Intel and AMD processors, AIX on IBM processors and IRIX on Silicon Graphics processors. Parallel processing directives are included in the code base through OpenMP. The ultimate goal of modeling GI electromagnetic phenomena using these visualizations is to provide an integrative framework for describing the physiological, anatomical and clinical knowledge of the GI system at the cellular (continuum) and macroscopic level.

In Section 2, functioning principles of the SQUID magnetometer and aspects of its architecture relevant to our program are presented. A description of the typical MGG experiment is also given in order to familiarize the reader with the manner in which biomagnetic signals are recorded from the human stomach and intestine.

The three major functional units of the data acquisition and analysis software are described in Section 3. These units – the data acquisition module, data processing and analysis module, and CMISS visualization module – are described in detail with respect to both their functionality and their design and implementation.

2. Instrumentation and experimental setup

A SQUID – superconducting quantum interference device – is a magnetometer that contains one or more Josephson junctions. A Josephson junction is a weak insulative layer between two superconductors that is able to support a supercurrent below a critical temperature I_c [27]. In a direct current (DC) SQUID – which contains two Josephson junctions – a superconducting loop with a pair of Josephson junctions is applied in order to measure the loop impedance. Due to several special properties of the Josephson junction, the impedance is a periodic function of the magnetic flux threading the SQUID. Using this setup, a modulation signal applied to the bias current and a lock-in detector are employed to measure the impedance and to linearize the voltage-to-flux relationship. Thus the SQUID functions as a flux-to-voltage converter of extremely high sensitivity. In biomagnetism, where the strength of the measured field is very weak and a substantial amount of information is present at low frequencies, the SQUID magnetometer is excellently suited as a measurement tool.

The Tristan 637i magnetometer has five pickup coils that record the magnetic field gradient in the $\hat{\mathbf{x}}$ direction and five coils for the $\hat{\mathbf{y}}$ direction. In addition, 19 axial coils are available for measuring gradients in the $\hat{\mathbf{z}}$ direction. The 29 superconducting pickup coils of the 637i SQUID magnetometer coils are distributed in the shape of two concentric, coplanar hexagons, as in Fig. 1, and can record the quantity $\Delta\mathbf{B}/\Delta z$. Ten other such input channels are also positioned in the same plane as the other channels, five of each being used to record $\Delta\mathbf{B}/\Delta x$ and $\Delta\mathbf{B}/\Delta y$, respectively. The 29 z channels of the SQUID measure

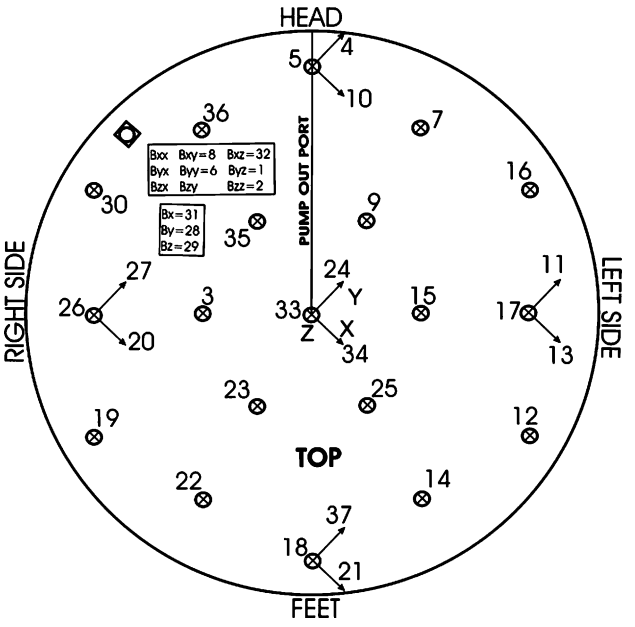

Fig. 1 – Spatial distribution of the co-planar input coils for the 637i SQUID biomagnetometer produced by Tristan Technologies (San Diego, CA). The magnetometer possesses a total of 29 pickup coils that are distributed within two concentric hexagons around a 5 cm baseline. Nineteen of these coils record changes in the magnetic field in the $\hat{\mathbf{z}}$ direction (i.e. $\Delta B_z/\Delta z$), while five coils record $\Delta B_x/\Delta x$ and five record $\Delta B_y/\Delta y$. The x and y channels are located at the center and extremities of the baseline and their positions are marked in the figure by short arrows inscriptioned with x or y, as appropriate. In addition to these 29 channels recording absolute changes in B_x, B_y and B_z, a number of noise channels and respiration channels for monitoring and recording breathholds are also provided.

only the $\mathbf{B}$ field component that is normal to the outer surface of the sensor and, because of the experimental setup for GI recordings, normal to the body of the subject. All three components of the field are measured at only five locations, thus allowing one to determine the direction of the field and its magnitude at those particular positions.

Once acquired by the SQUID, conditioned analog data are passed to a 3.5 GHz Pentium IV computer with 1 GB of RAM, using two PCI 6031E, 16 bit data acquisition cards as well as two SCB-100 connector blocks, all from National Instruments (Austin, TX). The data acquisition cards are controlled by in-house virtual instrument (VI) routines created solely for this application using Labview 6.0 (National Instruments, Austin, TX).

To insure time-aligned data acquisition from the two cards, a digital trigger is sent from one card to the other to start the acquisition process at the same time. Acquired data are lowpass-filtered at a cutoff frequency of 30 Hz using a finite impulse response (FIR) software filter. Writing data to disk at 3 MHz is prohibitive because of storage capacity issues; for this reason, acquired data are decimated by a factor of 10 and the effective sampling rate is thus reduced to 3 kHz before data are saved to disk.

3. Data acquisition, processing and analysis

A variety of hardware and software tools are required to record, decimate, filter and store SQUID data. Likewise, the analysis of GI electromagnetic phenomena from these recordings can be complex and time-consuming. Quite often, a large number of computational and visual tools are required to study and understand gastric ECA from magnetic field recordings. Because of this, any acquisition and analysis software for SQUID data must be flexible and adaptable; moreover, the nature and purpose of the analysis tools required for ECA analysis can differ quite significantly from study to study because their investigative goals can be very different. For all these reasons, a modular approach was adopted for the design of the acquisition and analysis program described in this article. Every module was designed separately with its own interface and visual features, while providing a unique control switchboard from which all modules can be easily accessed.

The first distinct unit of the program, the data acquisition module, is responsible for controlling data acquisition, analog filtering and storage in digital binary format. This module was designed in the LabView visual programming language and possesses a friendly GUI that allows data to be acquired easily and efficiently. The second unit, the data processing and analysis module, gives access to a number of important computational and visual tools whose use is very common in the analysis of GI magnetic signals. Such tools include data display and filtering, time–frequency representations (TFRs) of power series distributions in GI signals and SQUID data frequency maps. This module was implemented in the MatLab programming language. The third and last unit of the program contains a three-dimensional (3D) realistic model of the human torso and internal organs. Within this model, magnetic field components measured by the SQUID are visualized in 3D at the locations where they were recorded, with the reconstructed body of the stomach rendered directly below the magnetometer channel array. This last module was designed using the CMISS simulation program of the Bioengineering Institute at the University of Auckland, New Zealand. Throughout the remainder of this section, each of these modules is described in detail and examples of data processed using the program are given.

3.1. *Software control switchboard*

Each module of the acquisition and analysis program can be accessed from the software control switchboard. The graphical user interface of the switchboard is presented in Fig. 2. It includes a button for loading the acquisition program, one for loading the data analysis program and another one for generating a CMISS visualization. For historical reasons related to the development of the two applications, the format for CMISS input files is different from that in which data are written to disk by the SQUID acquisition module. An intermediate step must therefore be carried out in which an appropriate format conversion is made. This action is performed by pressing the third button visible on the switchboard.

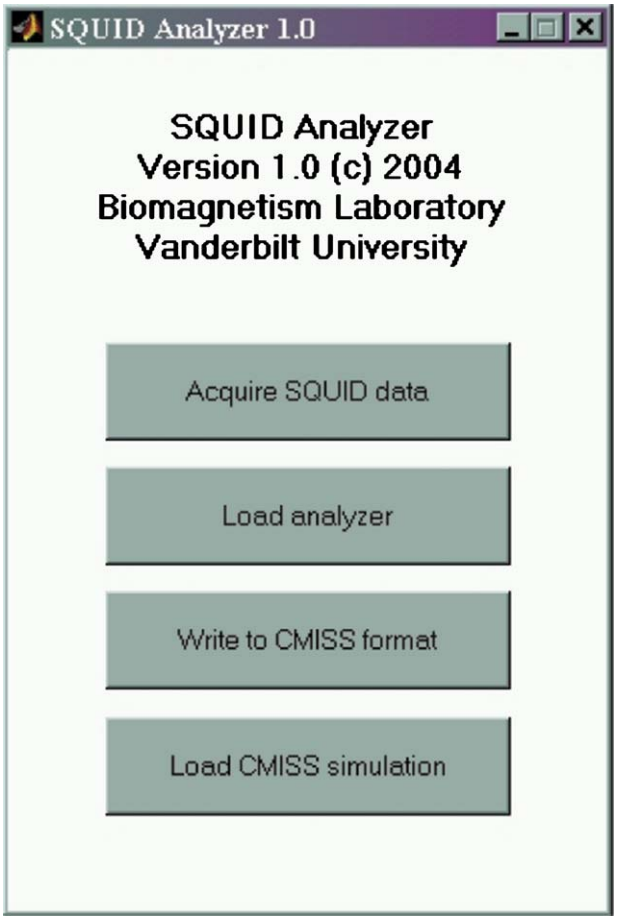

Fig. 2 – Software control switchboard for the acquisition and analysis program. The first button loads the LabView data acquisition module, while the second one is used for the data analysis and processing module. SQUID data can be converted into CMISS format using the third button, whereafter the CMISS visualization can be created.

3.2. *Data acquisition module*

The GUI used throughout the data acquisition process was developed using the LabView visual programming language; a sample screenshot is displayed in Fig. 3. As data is being acquired with the SQUID magnetometer, the signal recorded in each channel is plotted as a function of time on the corresponding graph labeled with the number of the appropriate channel. This allows one to observe and study SQUID data in real time as they are being acquired.

The SQUID magnetometer records analog signals at a DC frequency of 1 MHz. The original signal is then amplified and decimated to a frequency of 3 kHz post-acquisition. Lower frequency noise sources that are due to the motion artifacts of metal objects can be seen in the noise reference channels of the magnetometer and canceled adaptively or filtered digitally. Once acquired, the 3 kHz data are stored digitally in binary format for further processing.

A number of other acquisition controls and options are also made available in the GUI of the data acquisition module, as shown in Fig. 4.

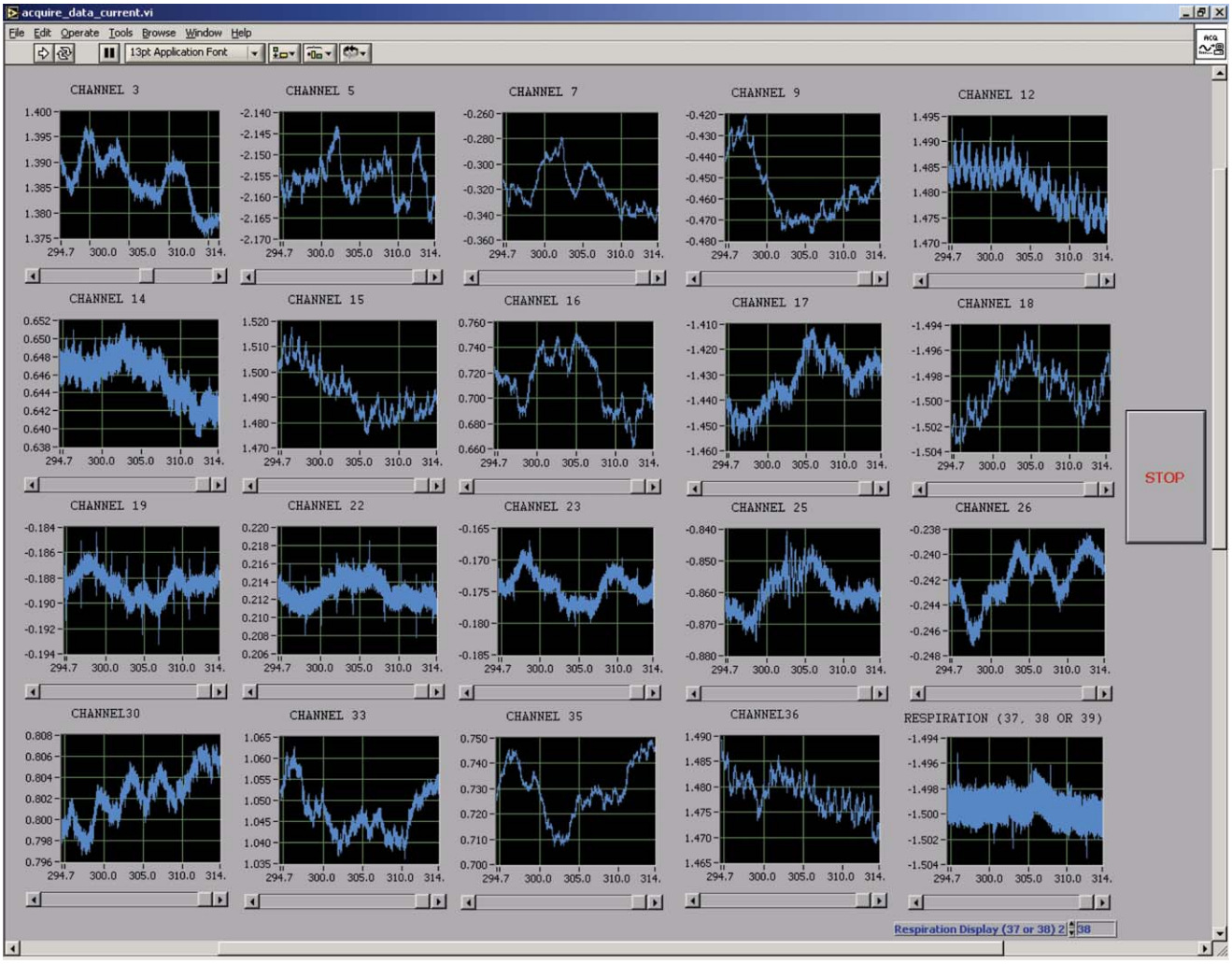

Fig. 3 – SQUID Analyzer GUI for the data acquisition module. The signal in every z channel is plotted against time using an adaptive technique where the interval range of the abscissa is varied with time according to the amplitude of the signal. In addition to vector sensor channels recording GI data, noise reference channels—e.g. channel 38, bottom right-used for noise cancellation can also be plotted.

3.3. *Data processing and analysis module*

A GUI was designed in MatLab for the data analysis module, dubbed SQUID Analyzer 1.0. The menu options of the GUI, `File`, `Data`, `Waterfall` and `Frequency`, allow the user to control the most important functions of the software. The first option from the `File` menu allows the user to open a raw data file created as a result of recording magnetic signals using the

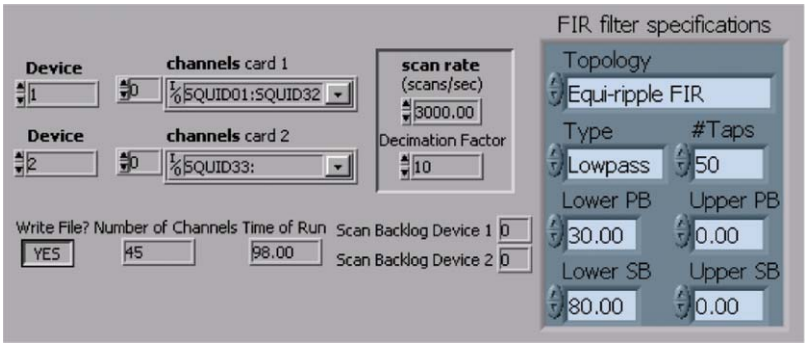

Fig. 4 – Control options for the data acquisition module of the SQUID Analyzer GUI. The data acquisition rate (scan rate), data decimation factor, FIR filter specifications and other options can be input here.

SQUID magnetometer; the user also has the option of loading only a smaller subset of channel data. Throughout the process of loading and decimating the data, a wait bar is displayed while the requested loading operation takes place. The SQUID Analyzer allows one to specify the decimation factor to be applied when loading the data; this can be an integer greater than or equal to 1.

3.4. *SQUID channel data visualization*

Several display options are made available from the `Data` menu. From the `Plot raw data` menu item, the user is given access to the two options of plotting raw data, labeled `Numerical channel order` and `Spatial channel arrangement`. These two display modes are also available from the second menu item, namely `Plot filtered data`. The third menu item, `Adjust data time range`, allows the user to focus only on a particular time segment within a data set, which is very useful because breathhold time intervals within a large data set can be processed and analyzed more adequately.

Two different display options are available for visualizing data acquired from the SQUID magnetometer. In the first of these, plots of electric potential or magnetic field data are shown in the numerical order of each channel. This view has two primary advantages. First of all, it provides an ordered display of data that is made available in a conventional manner. Secondly, it allows one to easily identify and analyze the data in a channel of interest simply from the numerical ordering of the channels.

The second data view provided attempts to reproduce the spatial arrangement of each input coil of the gradiometer (see Fig. 5). This view has the advantage of providing a way to associate each data channel with a particular anatomic region of interest. It also allows one to identify areas where particular frequencies in the electrical activity signal are present. This can be useful because, very often, a specific frequency value can allow one to associate the region where that frequency component is strongest with a particular organ, e.g. with a particular segment of the intestine. Moreover, it may be possible to observe and analyze the frequency gradient of the ECA along the GI tract from the visual analysis of SQUID data being displayed in this fashion. The spatial arrangement mode is adapted to the configuration of the Tristan 637i biomagnetometer, but the program can be easily adapted for different coil positions.

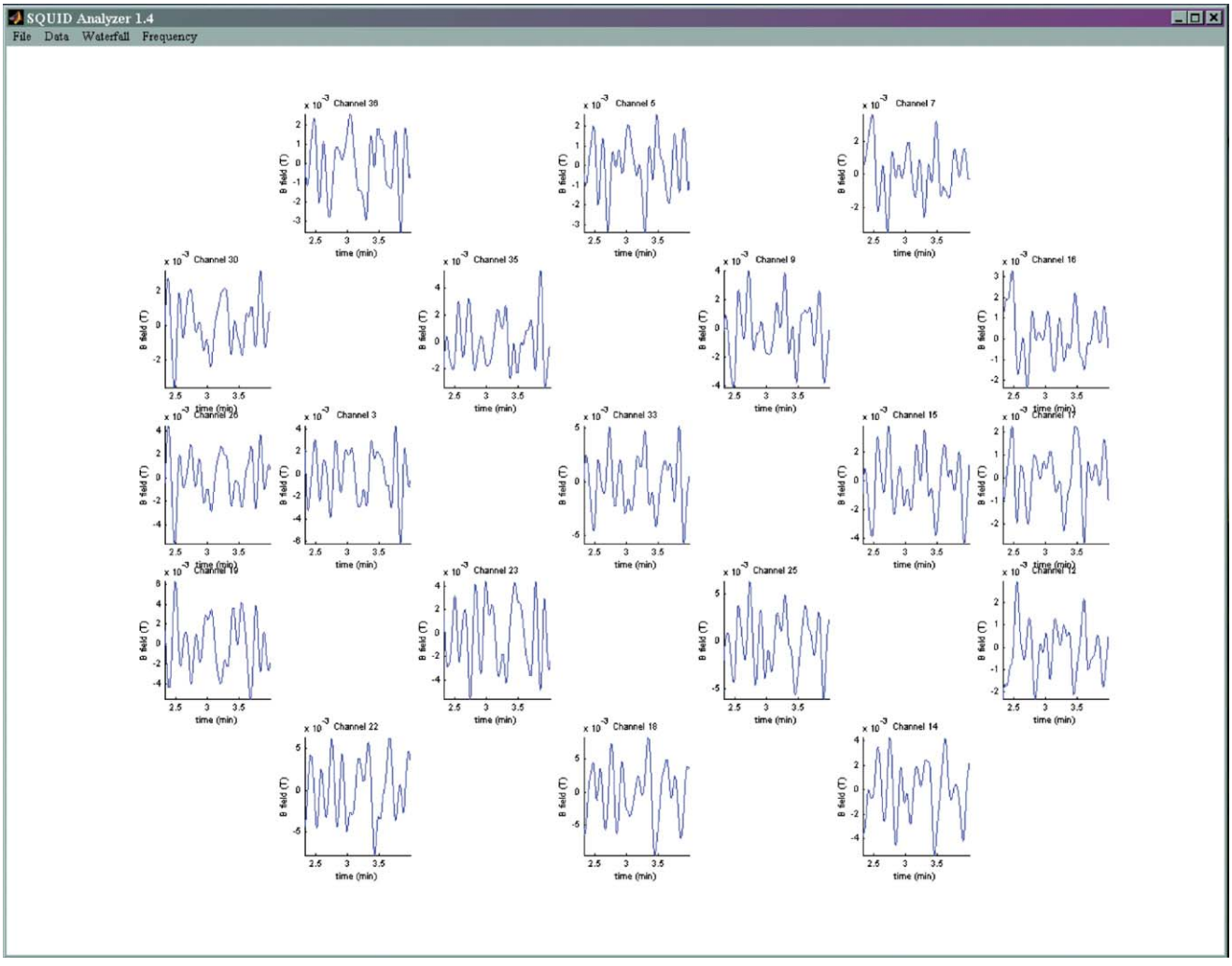

Fig. 5 – Sample filtered SQUID z channel data displayed using the spatial arrangement of the magnetometer's z channels.

The second item from the Data menu gives the user access to the data filtering features of the program. The first data processing step involves detrending the data; this is done to eliminate undesired, short-lived trends in the data by removing the mean value or linear trend from a vector or matrix in view of FFT processing. It computes the least-squares fit of a straight line (or composite line for piecewise linear trends) to the data and subtracts the resulting function from the data.

Noise with a frequency lower than 1.5 cpm is then subtracted by the software using polynomial subtraction of variable order, in which a polynomial is fit to short-lived trends in the data and then subtracted from it to remove these trends. The degree of the polynomial is user-selectable. The third data processing step involves the design of a bandpass, second-order Butterworth filter. The Butterworth filter is maximally flat in the pass band and monotonic overall, which reduces the effect of pass band ripples in the signal to a minimum. Such a filter sacrifices rolloff steepness for monotonicity in the pass- and stopbands. The function used by our software creates z-transform coefficients for a Butterworth filter up to a user-defined order. These coefficients are used to filter the data in the forward and reverse directions for zero-phase filtering. This is done by processing the input data in both the forward and reverse directions [23]; after filtering in the forward direction, the filtered sequence is reversed and run back through the filter. The resulting sequence has precisely zero-phase distortion and double the filter order. Zero-phase distortion is necessary in our case because it avoids the distortion of magnetic field propagation characteristics. In addition to the forward–reverse filtering, our software minimizes startup transients by adjusting initial conditions to match the DC component of the signal and by prepending several filter lengths of a flipped, reflected copy of the input signal [19].

The default filter cutoff frequencies specified by the SQUID Analyzer software program are 1.8 and 18 cpm, corresponding to 0.03 and 0.3 Hz, respectively. While the GEA has a frequency of approximately 3 cpm, intestinal activity exhibits a frequency gradient along the GI tract and its frequencies range between approximately 4 and 18 cpm. Thus, the default parameters of the program are adequate for capturing information contained in the signal that refers to these two phenomena.

In clinical GI research, changes in the frequency components of the signal are of interest. To study those, power spectral density (PSD) estimates for each of several epochs in the signal must be computed to create a time–frequency representation of the data [3,4]. Two methods for carrying out this task are most common: the classical fast Fourier transform (FFT) and modern autoregressive (AR) spectral analysis. The Fourier power spectrum is very suitable for stationary signals that are not expected to change over the duration of the sample. Because FFT spectral resolution increases with the length of the sample – thus requiring long sample durations for better resolution – this method is not optimal for studying ischemic signals, which are prone to change over short periods of time. For this reason, AR spectral analysis is preferable for short time intervals (1 min). Although efficient and accurate, AR spectral analysis also suffers from a number of drawbacks. For a sinusoidal wave, the area under the AR spectral curve depends on the signal power in a linear fashion, but peaks in the AR PSD are proportional to the square of the power [18]. Deviations of real signals from sinusoids also make the problem of estimating amplitudes more problematic [4]. For this reason, the square root of the AR PSD is often reported. Thus AR analysis is an inappropriate tool for determining the power at given frequencies, although it is certainly useful for locating dominant frequencies in the sample. For further information and comparison of AR and FFT analyses, we direct the reader to [26].

In light of these two alternative, both AR analysis and the FFT are included in our software. The frequency spectra of the analyzed signal can be computed by the SQUID Analyzer using the fast Fourier transform to obtain power spectral density values for a specific frequency range. First, segments of data each containing one minute of SQUID recordings are created. Every segment is then windowed using a Hanning window to reduce FFT leakage error and zero-padded to increase frequency sampling in the spectrum. The FFT of the signal is then computed and the resulting frequency spectra are assembled for all data segments and displayed in the form of a three-dimensional frequency spectra waterfall plot, where each plot corresponds to one minute of SQUID data. A wait bar is displayed to the screen while this process is applied to the loaded data. As in the case of raw data display, a numerical order and a spatial arrangement display mode are made available for waterfall plots. When accessing either one of these, an input box is displayed, prompting the user to specify the cutoff frequencies to be used as parameters to the filter.

Although data trends due to extraneous causes are removed by detrending, it can often be difficult to analyze and understand such data due to its high time variability and to the large time interval used for display on the ordinate axis. To correct this inconvenience and to provide a more reliable tool for analysis, the Adjust data time range option was made available from the Data menu. When accessing this option, an input box is displayed to the screen; the user can then input the time interval in seconds for which data is to be displayed. This feature is useful because, very often, for example, waveforms that are of biophysical interest are easier to view and analyze on a minute-by-minute basis as opposed to the alternative of viewing the entire dataset at once. As is apparent from this figure, all the waveforms are much easier to analyze and interpret when a smaller time interval is used for display.

3.5. *MGG waterfall plot generation*

In addition to displaying raw and filtered SQUID channel data, the SQUID Analyzer is equipped with the ability to create waterfall plots of GI signal frequency spectra. As explained previously, these spectra are computed using the FFT.

The display options available for frequency waterfall plots are similar to those for visualizing raw or filtered data. Each plot can be viewed either in the numerical order of the magnetometer channels or using the spatial arrangement setup in which every waterfall plot is at the approximate location of the corresponding SQUID input coil (Fig. 6). In addition, a number of options are made available to manipulate the waterfall plots three-dimensionally. By pressing the ↑ and ↓ keys, the elevation of the camera viewpoint for each waterfall plot

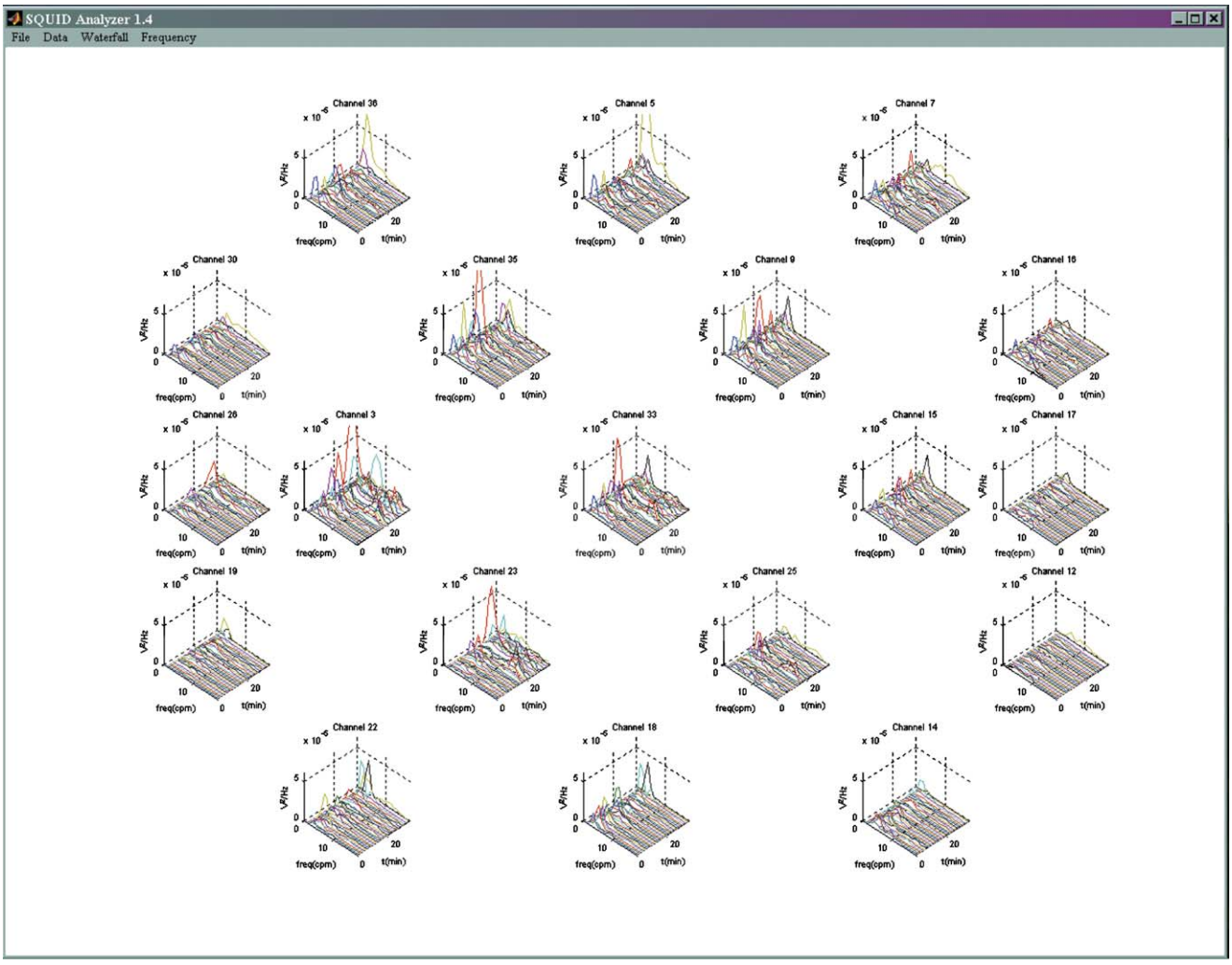

Fig. 6 – Sample waterfall plots generated using the spatial channel arrangement display mode. The dominant frequency of 3 cpm due to the gastric signal can be seen in each channels.

can be increased or decreased, respectively, by increments of 5° in the range −90° to 90°. Similarly, pressing the ← or → keys changes the azimuth of the viewpoint by decrements or increments of 5°, respectively, in the range 0–360°.

Other display options associated with the frequency waterfall plots include spectra normalization, changing grid visibility and the modification of the $\hat{\mathbf{z}}$ axis range displayed in each waterfall plot. When the spectra normalization option is used, every point in each 3D waterfall plot is normalized to the absolute maximum in that plot and this process is repeated for all the waterfall plots displayed. Changing grid visibility, on the other hand, removes or redraws the coordinate grid of each plot, as appropriate.

3.6. *Frequency map creation*

The third important functionality of the SQUID Analyzer is to produce SQUID data frequency plots. The purpose of this is to associate the frequency spectrum data presented in waterfall plots with the spatial locations of the SQUID input coils. Spatial maps of frequency content allow one to localize electrical activities with different frequencies, such as the higher frequencies of small bowel electrical activity or brady- and tachygastrias.

The creation of frequency plots relies on the filtering and FFT frequency spectra computation processes that have already been described. To generate these plots, the frequency spectra are divided into segments of variable length spanning the frequency interval specified by the cutoff frequencies of the Butterworth filter. For instance, consider a spectrum generated as a result of applying the FFT to a dataset that has been filtered using a Butterworth filter with cutoff frequencies of 1 and 15 cpm. Such a spectrum can be divided into segments spanning one cpm, i.e. 1–2 cpm, 2–3 cpm, ..., 14–15 cpm. For each such interval of the form $[t_{i-1}, t_i]$ among the entire set of frequency spectrum intervals $[t_0, t_1], [t_1, t_2], \ldots, [t_{n-1}, t_n]$, one can compute the definite integral

$$\int_{t_{i-1}}^{t_i} f(x)\,dx, \tag{1}$$

where $f(x)$ is the PSD function. This process can be repeated for each SQUID input channel and the value of the integral

can be associated with the spatial location of the respective channel.

These values can then be interpolated on a 2D grid within the area delimited by the SQUID input coil perimeter. Thus, one can generate a 3D surface that represents a mapping of frequencies within the SQUID coil perimeter. Such a surface is in effect a function of two coordinate variables (x and y) that allows one to associate a particular frequency with a specific spatial location. In this manner, anatomical regions of the body can be associated with certain frequencies and regions where a particular frequency is dominant can be easily identified from the frequency map. The process described above can be repeated for each time interval of SQUID data being analyzed; an example of the results obtained for one such time interval is presented in Fig. 7.

3.7. *CMISS visualization module*

The third module of the SQUID Analyzer program was implemented in CMISS. The anatomical data source that was used for the construction of the initial GI model is the Visible Human Project [25]. The image set provided by this project was used to extract data points which were then used to fit an initial generic model to the data via an optimization algorithm in which distances between points in the data and fitted models was minimized [24]. From this initial data, a bilinear surface mesh was created and refitted using the iterative fitting procedure of Bradley et al. [2] to generate a bicubic Hermite C^1 mesh. This procedure was used for all internal organs, including the small and large intestines. For the stomach, the muscular microstructure was added because the directions of electrical

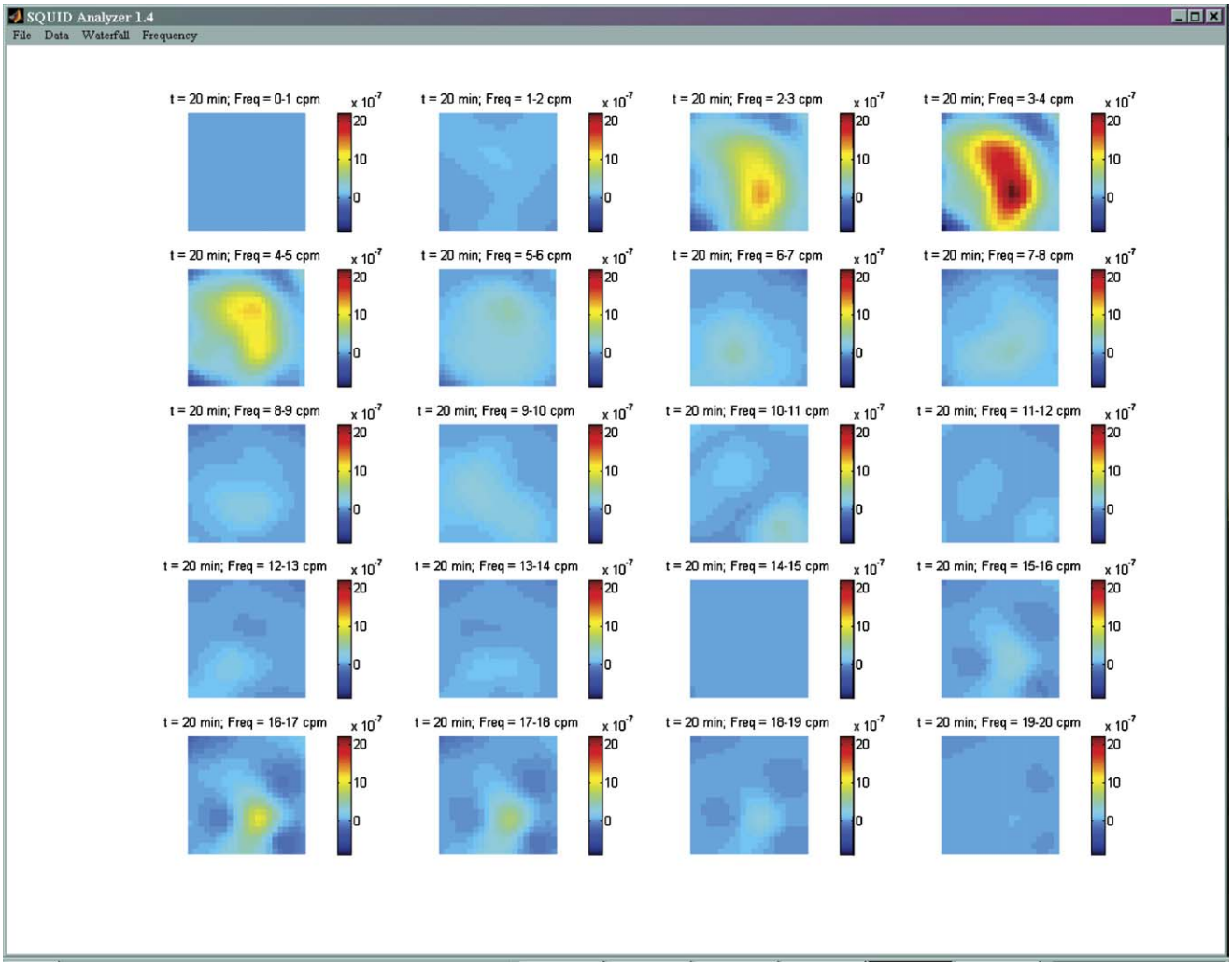

Fig. 7 – Sample frequency maps generated using SQUID Analyzer 1.0. Frequency data within the spatial extent of the biomagnetometer input coils is represented continuously using a data grid interpolation algorithm. The frequency spectrum is divided into intervals of one cycle per minute each and the corresponding frequency data is used to generate the frequency maps. This is done for the time data points provided in the input file such that one set of frequency maps corresponds to one minute of GI electrical activity contained in the SQUID input data file. In the figure above, the signal with the highest magnitude is evident in the 3–4 cpm range and its location can be identified as the anatomic region of the stomach using the frequency map technique. All maps are drawn to the same scale – as can be seen from the colorbar limits – and the PSD values plotted are dimensionless.

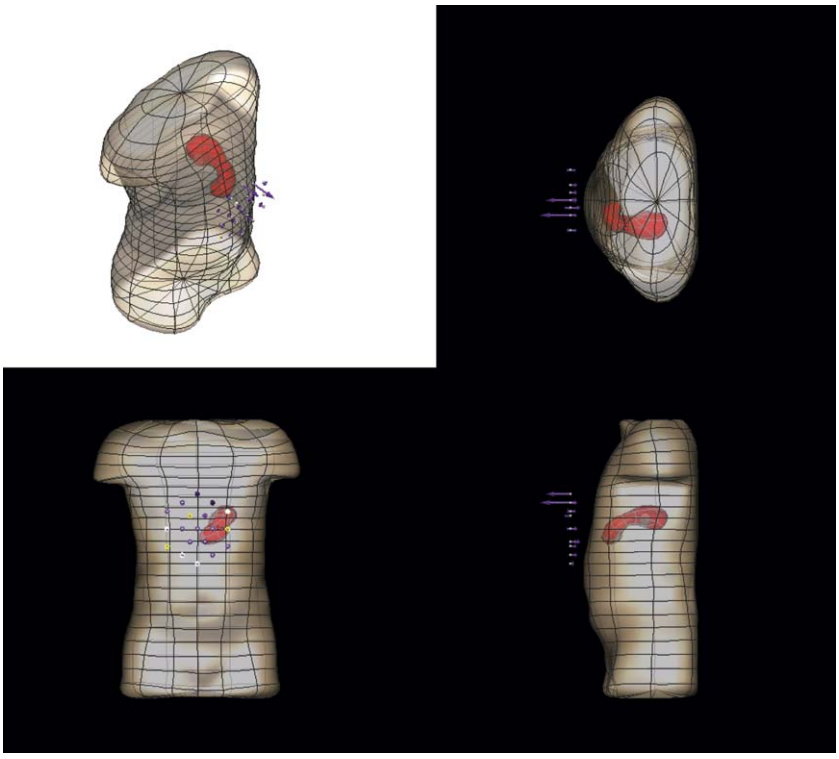

Fig. 8 – Perspective viewpoints available from the CMISS simulation. In the top-left white rectangle, the viewpoint of the camera can be changed by dragging the mouse over the screen. The viewpoint in the other three rectangles cannot be changed, allowing the user to have a frontal, lateral and upper view of the torso and SQUID input locations at the same time.

propagation and contraction are often preferential [24,8,10]. The thickness of organ walls was added to each digestive organ by internal projection of the outer surface towards the mesh centerline. For the stomach, five layers were included in the model: a longitudinal layer, a thin ICC layer, a circular muscle layer, a second thin ICC layer and a second circular muscle layer [24]. The assumption of transverse anisotropy was made and a microstructural fiber direction was described in each smooth muscle layer.

Because the spatial scale of the finite elements fitted from the digitized data is too coarse to solve the bidomain equations, a finite element finite difference method or a structured finite element method was employed [6,11]. To create a 3D animation of magnetic field vectors, SQUID signal data output by the magnetometer and written to the storage medium must be converted into a format compatible with CMISS. This can be done from the software control switchboard, as previously explained.

An example of the visualizations produced by CMISS is presented in Fig. 8, where the body of the stomach is simulated within the torso. Above the abdomen, each location of the SQUID magnetometer input coils is represented by a small dot. For each corresponding input channel, a purple vector arrow is drawn to represent the quantity B_z recorded in that respective SQUID channel.

As Fig. 8 shows, several views are available for this simulation. In the top-left white rectangle, the viewpoint of the camera can be changed by dragging the mouse over the screen. The viewpoint in the other three rectangles cannot be changed, allowing the user to have a frontal, lateral and upper view of the torso and SQUID input locations at the same time.

Magnetic field data acquired with the SQUID can be related to a model of the patient, or overlain on a generic torso. To incorporate a patient specific model, appropriate anatomical images (CT/MRI) must firstly be acquired, together with appropriate information with respect to the location of the patient with respect to the SQUID sensors. A model of the patient (complete with representations of the stomach and small intestine, if desired) can then be constructed using the methods outlined in [24]. For the information displayed here, a generic torso model, based on the Visible Human Project, was used.

The GUI available in CMISS for controlling the parameters of the simulation allows one to see all or only a selection of available view modes. The user can also take a screenshot of the visualization window and save the resulting image to any storage medium. Because one frame is generated for each minute of data, a set of tools are provided to access different frames. One of these is a slidebar which can be used to visualize different display frames of the simulation. Alternatively, the entire movie can be played in an infinite loop. A perspective image of the torso can be obtained and seven other views can also be selected.

4. Conclusion

The reliability of data analysis tools can be crucial to the process of making appropriate interpretations of experimen-

tal data and to the ultimate success or failure of any scientific investigation. This is why the development of our package marks a positive step in improving GI clinical diagnosis. Because very little software development for the field of GI biomagnetic research has been done up to this point, our modular program contributes to the establishment of the MGG as a trustworthy investigative method. The modular approach adopted for the development of the SQUID Analyzer software program also implies the ability of our integrated analysis tool to undertake further development. Thus far, the use of waterfall plots and frequency maps for GI data analysis has become a standard in many physiological studies [5]. Our CMISS visualization tool, on the other hand, is novel to the modeling of the GI system, although it borrows heavily in ideas and character from similar methodologies that are available for cardiac modeling and simulation. This exchange of techniques between the two areas is useful in light of the experience that already exists in the cardiac field; this historical background is relevant because much of the electrodynamics that is now only beginning to be investigated in GI research already benefits from over 20 years of study in cardiac modeling.

Much future development can be undertaken in the direction outlined in this article. Although many signal analysis concepts that are potentially useful in GI electrodynamics are not discussed here, the modular structure of the SQUID Analyzer program allows much more to be implemented. For example, an important area whose history of investigation in cardiac research is extensive concerns the biomagnetic inverse problem and the information that inverse solutions can yield concerning the patterns of (ab)normal current propagation in the GI tract. Filtering and signal processing methods remain another area of improvement, particularly with the recent implementation of wavelet and independent component analysis to the field of GI research [14,16]. Chaos analysis methods are another set of tools that deserve to be incorporated, especially since GI pathology seems to be associated with changes in chaos patterns in diseased individuals [21]. One feature that our interface lacks is the ability to compare the realism of various theoretical models of GI phenomena based on experimentally acquired data. This may become important in the near future as more attention has been recently devoted to GI modeling in the context of conoidal and ellipsoidal geometry [20,12,13].

Acknowledgements

The authors are grateful to M.R. Gallucci and R.L. Palmer (Department of Surgery, Vanderbilt University School of Medicine, Nashville, TN) and to J.A. Sims (Department of Biomedical Engineering, University of North Carolina, Chapel Hill, NC) for their useful suggestions. A.J.P. is the recipient of a James Cook research fellowship and L.K.C. is supported from a Marsden fund, both from the Royal Society of New Zealand. Both New Zealand and US groups are funded by the US National Institute of Health, grants R01 DK 54775, 58697 and 58197.

REFERENCES

[1] W.C. Alvarez, The electrogastrogram and what it shows, J. Am. Med. Assoc. 78 (1921) 1116–1119.
[2] C.P. Bradley, A.J. Pullan, P.J. Hunter, Geometric modeling of the human torso using cubic Hermite elements, Ann. Biomed. Eng. 25 (1997) 96–111.
[3] L.A. Bradshaw, S.H. Allos, J.P. Wikswo Jr., W.O. Richards, Correlation and comparison of magnetic and electric detection of small intestinal electrical activity, Am. J. Physiol. Gastrointestinal Liver Physiol. 272 (1997) G1159–G1167.
[4] S.H. Allos, D.J. Staton, L.A. Bradshaw, S. Halter, J.P. Wikswo Jr., W.O. Richards, Superconducting quantum interference device magnetometer for diagnosis of ischemia caused by mesenteric venous thrombosis, World J. Surg. 21 (1997) 173–178.
[5] L.A. Bradshaw, A.G. Myers, A. Redmond, J.P. Wikswo Jr., W.O. Richards, Biomagnetic detection of gastric electrical activity in normal and vagotomized rabbits, Neurogastroenterol. Motility 15 (2003) 475–482.
[6] M.L. Buist, G.B. Sands, P.J. Hunter, A.J. Pullan, A deformable finite element derived finite difference method for cardiac activation problems, Ann. Biomed. Eng. 31 (2002) 577–588.
[7] CMISS: An interactive computer program for Continuum Mechanics, Image analysis, Signal processing and System Identification, http://www.cmiss.org., accessed July 13, 2004.
[8] E.E. Daniel, Y.F. Wang, Gap junctions in intestinal smooth muscle and interstitial cells of Cajal, Microsc. Res. Technol. 47 (1999) 309–320.
[9] J.E. Everhart, Digestive diseases in the United States: epidemiology and impact, U.S. Department of Health and Human Services, National Institutes of Health, National Institute of Diabetes and Digestive and Kidney Diseases, U.S. Government Printing Office, Washington, DC, 1994.
[10] G.D.S. Hirst, An additional role for ICC in the control of gastrointestinal motility? J. Physiol. 537 (2001) 1.
[11] D.A. Hooks, Three-dimensional mapping of electrical propagation in the heart: experimental and mathematical model based analysis, Ph.D. Thesis, The University of Auckland, New Zealand, 2001, pp. 26–33.
[12] A. Irimia, L.A. Bradshaw, Theoretical ellipsoidal model of gastric electrical control activity propagation, Phys. Rev. E: Stat. Nonlinear Soft Matter Phys. 68 (2003) 051905.
[13] A. Irimia, L.A. Bradshaw, Ellipsoidal electrogastrographic forward modelling, Phys. Med. Biol. 50 (2005) 4429–4444.
[14] A. Irimia, L.A. Bradshaw, Artifact reduction in magnetogastrography using fast independent component analysis, Physiol. Meas. 26 (2005) 1059–1073.
[15] The International Union of Physiological Sciences, http://www.iups.org., accessed July 15, 2004.
[16] S. Kara, F. Dirgenali, Okkesim Ş, Estimating gastric rhythm differences using a wavelet method from the electrogastrograms of normal and diabetic subjects, Instrum. Sci. Technol. 33 (2005) 519–532.
[17] K.L. Koch, Diabetic gastropathy: gastric neuromuscular dysfunction in diabetes mellitus. A review of symptoms, pathophysiology and treatment, Dig. Dis. Sci. 44 (1999) 1061–1075.
[18] S.L. Marple, Digital Spectral Analysis with Applications, Prentice Hall, Englewood Cliffs, New Jersey, 1987.
[19] MatLab 6.0 Help Manual Version 12.1, Mathworks Inc., Nantucket, Massachusetts, 2003.
[20] M.P. Mintchev, K.L. Bowes, Conoidal dipole model of electrical field produced by the human stomach, Med. Biol. Eng. Comput. 33 (1995) 179–184.
[21] M.P. Mintchev, A. Stickel, K.L. Bowes, Dynamics of the level of randomness in gastric electrical activity, Dig. Dis. Sci. 43 (1998) 953–956.

[22] D. O'Donovan, C. Feinle-Bisset, K. Jones, M. Horowitz, Idiopathic and diabetic gastroparesis, Curr. Treat. Options Gastroenterol. 6 (2003) 299–309.
[23] A.V. Oppenheim, R.W. Schafer, Discrete-Time Signal Processing, Prentice-Hall, 1989, pp. 311–312.
[24] A. Pullan, L. Cheng, R. Yassi, M. Buist, Modeling gastrointestinal bioelectric activity, Prog. Biophys. Mol. Biol. 85 (2004) 523–550.
[25] V. Spitzer, M.J. Ackerman, A.L. Scherzinger, R.M. Whitlock, The visible human male: a technical report, J. Am. Med. Inform. Assoc. 3 (1996) 118–130.
[26] G.K. Turnbull, S.P. Ritcey, G. Stroink, B. Brandts, P. van Leeuwen, Spatial and temporal variations in the magnetic fields produced by human gastrointestinal activity, Med. Biol. Eng. Comput. 37 (1999) 549–554.
[27] J.P. Wikswo Jr., SQUID magnetometers for biomagnetism and nondestructive testing: important questions and initial answers, IEEE Trans. Appl. Supercond. 5 (1995) 74–80.